

*Short Communication*

## **Anemone-shaped Fe<sub>3</sub>O<sub>4</sub> Micro-structures as the Anode Materials in High Electrochemical Performance Li-ion Batteries**

Hui Lv\*, Xiaohui Feng, Haidan Bi, Xinli Song

College of Food Science and Pharmaceutical Engineering, Zaozhuang University, Zaozhuang 277160, China

\*E-mail: [Lvhui2016@163.com](mailto:Lvhui2016@163.com)

*Received:* 3 March 2022 / *Accepted:* 14 April 2022 / *Published:* 7 May 2022

Self-assembled anemone-shaped Fe<sub>3</sub>O<sub>4</sub> micro-structures were synthesised via a facile solvo-thermal method. The crystalline structure and micro appearance of the obtained crystals were characterised via X-ray diffraction, transmission electron microscopy and scanning electron microscopy. The as-obtained anemone-shaped Fe<sub>3</sub>O<sub>4</sub> micro-structures comprised nano-rods, approximately measuring 300–400 nm in diameter. The electrochemical performances of the anemone-shaped Fe<sub>3</sub>O<sub>4</sub> micro-structures were evaluated via cyclic voltammetry, galvanostatic cycling tests and electrochemical impedance spectroscopy. The pure-phase anemone-shaped Fe<sub>3</sub>O<sub>4</sub> micro-structures exhibited a large reversible capacity of 556 mAh g<sup>-1</sup> after 100 cycles at 100 mA g<sup>-1</sup>, which is 48% retention of the initial reversible capacity (1166 mAh g<sup>-1</sup>) and good rate capability. These results demonstrate the potential use of self-assembled anemone-shaped Fe<sub>3</sub>O<sub>4</sub> micro-structures as promising anode materials for developing Li-ion batteries.

**Keywords:** Anemone-shaped Fe<sub>3</sub>O<sub>4</sub> micro-structures; Electrochemical measurement; Anode material; Li-ion battery

### **1. INTRODUCTION**

Magnetite (Fe<sub>3</sub>O<sub>4</sub>) has been extensively studied as an electrode material in Li-ion batteries because of its environmental safety, low cost and high theoretical capacity (926 mAh g<sup>-1</sup>) [1-4]. Wu et al. reported that self-assembled Fe<sub>3</sub>O<sub>4</sub> hierarchical micro-spheres as superior anode materials for Li-ion batteries showed a high specific capacity of >1000 mAh g<sup>-1</sup> at 0.5 A g<sup>-1</sup> after 270 cycles and excellent cycling stability [5]. Choi et al. prepared Fe<sub>3</sub>O<sub>4</sub> thin films as anode materials in Li-ion batteries for simultaneously exhibiting a high reversible Li<sup>+</sup> capacity with excellent cycling performance for Li-ion batteries (only 8% loss after 100 cycles) [6]. Various nano-structures, such as one-dimensional Fe<sub>3</sub>O<sub>4</sub>

sub-micro fibres, self-assembled submicron spheres, flower-like meso-porous Fe<sub>3</sub>O<sub>4</sub> and hollow Fe<sub>3</sub>O<sub>4</sub> micro-spheres, have been developed for improving the performance of Fe<sub>3</sub>O<sub>4</sub> electrodes for Li-ion batteries [7-10]. Various shapes nano-structure fabrication helps enhance the rate and cycling performance of electrodes in Li-ion batteries.

In the present study, a facile solvo-thermal method was designed for fabricating self-assembled anemone-shaped Fe<sub>3</sub>O<sub>4</sub> micro-structures. Electrochemical studies showed that the self-assembled anemone-shaped Fe<sub>3</sub>O<sub>4</sub> micro-structures exhibited high reversible capacity (1166 mAh g<sup>-1</sup>) and excellent cycle performance (556 mAh g<sup>-1</sup> retention after 100 charge–discharge cycles at 100 mA g<sup>-1</sup>) as Li-ion battery materials. In addition, the Coulombic efficiency of anemone-shaped Fe<sub>3</sub>O<sub>4</sub> exceeded 99% after 100 cycles.

## 2. EXPERIMENTAL DETAILS

In a typical synthesis of the self-assembled anemone-shaped Fe<sub>3</sub>O<sub>4</sub> micro-structures, hexahydrated ferric chloride (5 mmol) and sodium acetate tri-hydrate (0.04 mol) were dissolved in 50 mL of ethylene glycol and continuously stirred magnetically for 30 min. Subsequently, 4 mL of ethylenediamine was added to the aforementioned solution. After vigorously stirring for 2 h at 30 °C, the mixture solution was transferred into a teflon-lined stainless steel autoclave (100 mL) and maintained at 220 °C for 16 h. The as-obtained self-assembled anemone-shaped Fe<sub>3</sub>O<sub>4</sub> micro-structures were retrieved using a magnet and repeatedly washed with absolute ethanol and deionised water. Subsequently, the products were vacuum-dried overnight at 50 °C before further processing.

The crystal structure and phase of the obtained materials were identified via the X-ray diffraction (XRD, Bruker AXS D8, CuK $\alpha$ ). The morphologies and micro-structure of the as-prepared products were examined via the scanning electron microscopy (SEM, Hitachi-S4800) and transmission electron microscopy (TEM, JEOL-JEM2100F, 200 kV).

The working electrodes for the electrochemical experiments were prepared by spreading a mixture of acetylene black (15 wt%), active materials (anemone-shaped Fe<sub>3</sub>O<sub>4</sub> micro-structures, 70 wt%) and a binder (PVDF, 15 wt%) dissolved in N-methyl pyrrolidone as a solvent onto a copper foil current collector using the doctor-blade method. After vacuum drying at 60 °C for 10 h, coin-type CR2032 cells with Li foils as the counter electrode were assembled in the argon-filled glove box with <1 ppm moisture and oxygen. A Celgard 2300 was used as the separator. The electrolyte contained 1-M LiPF<sub>6</sub> dissolved in ethylene carbonate/ethylmethyl carbonate/dimethyl carbonate (EC/EMC/DMC, 1:1:1 in weight ratio). The rate capability and cycling life of the cells were evaluated using a battery analyser between 0.01 and 3.00 V (vs. Li<sup>+</sup>/Li). Cyclic voltammetry (CV) was conducted at a scan rate of 0.1 mV s<sup>-1</sup> between 0.01 and 3.00 V using a CHI660E instrument. The electrochemical kinetics of anemone-shaped Fe<sub>3</sub>O<sub>4</sub> was examined via the electrochemical impedance spectroscopy (EIS) on an electrochemical workstation (Solartron 1287) with an AC amplitude of 5 mV in the frequency range of 100 kHz–0.01 Hz.

### 3. RESULTS AND DISCUSSION

The phase and structure of the self-assembled anemone-shaped  $\text{Fe}_3\text{O}_4$  micro-structures were examined via the XRD (Fig. 1). The XRD peaks of the self-assembled anemone-shaped  $\text{Fe}_3\text{O}_4$  micro-structures were assigned to a pure magnetite spinel cubic phase of  $\text{Fe}_3\text{O}_4$  [space group:  $\text{Fd}\bar{3}\text{m}$  (227)], which was indexed to the pure phase of  $\text{Fe}_3\text{O}_4$  (JCPDS No.65-3107) [11,12]. Only narrow and sharp XRD peaks of  $\text{Fe}_3\text{O}_4$  were observed, demonstrating the good crystalline nature and phase purity of  $\text{Fe}_3\text{O}_4$ .

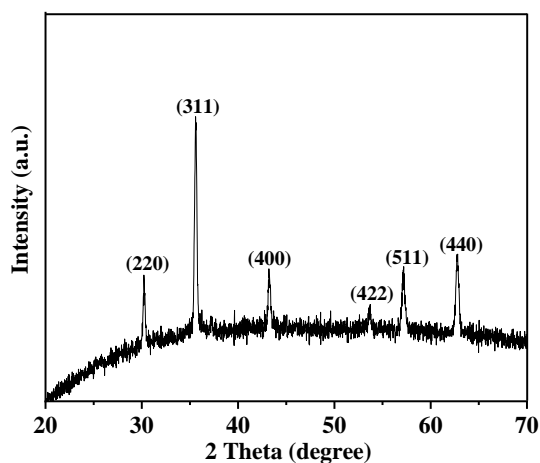


**Figure 1.** XRD pattern of the anemone-shaped  $\text{Fe}_3\text{O}_4$  micro-structures.

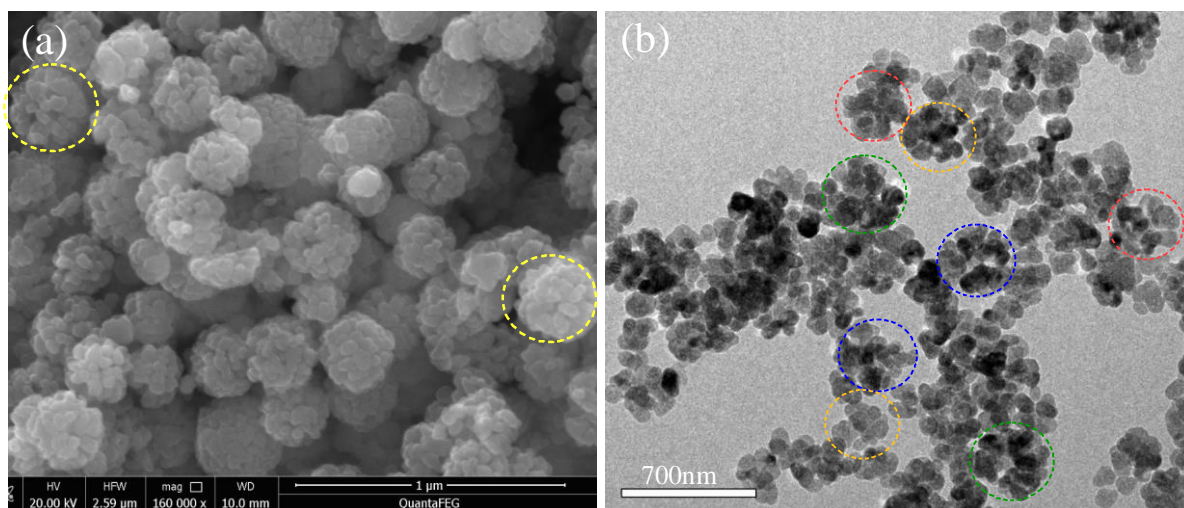


**Figure 2.** SEM (a) and TEM (b) images of the anemone-shaped  $\text{Fe}_3\text{O}_4$  micro-structures.

The general micro-morphology of the as-obtained products was observed via the SEM and TEM (Fig. 2). The anemone-shaped  $\text{Fe}_3\text{O}_4$  micro-structures were assembled from nano-rods, approximately measuring 300–400 nm in diameter (Fig. 2 (a)). The self-assembled anemone-shaped

Fe<sub>3</sub>O<sub>4</sub> micro-structures were observed via the TEM (Fig. 2 (b)), which clearly showed that the anemone-shaped Fe<sub>3</sub>O<sub>4</sub> micro-structures comprised Fe<sub>3</sub>O<sub>4</sub> nano-rods with their one-side inserted the inner.

CV profiles of the anemone-shaped Fe<sub>3</sub>O<sub>4</sub> micro-structures electrode for the first five cycles were obtained at a scan rate of 0.1 mV s<sup>-1</sup> over the voltage range of 0.01–3 V (Fig. 3 (a)). During the first cycle, anemone-shaped Fe<sub>3</sub>O<sub>4</sub> exhibited a strong cathodic peak at approximately 0.60 V. This can be ascribed to the reduction of active material to Fe and the formation of amorphous Li<sub>2</sub>O [13]. In the charging process, the broad oxidation peaks at approximately 1.69 V correspond to the reversible oxidation (Fe<sup>0</sup> → Fe<sup>2+</sup>/Fe<sup>3+</sup>) during the anodic processing. For the subsequent cycles, the oxidation and reduction peaks shifted to approximately 1.73 and 0.76 V during charge and discharge, respectively, owing to polarisation of the electrode material [14]. Complex reactions between the electrolyte interface and the electrode occur to form the solid-electrolyte interphase (SEI) layer on the active materials [15,16]. Moreover, the CV curves in the following cycles decreased slightly, indicating low capacity fading of the anemone-shaped Fe<sub>3</sub>O<sub>4</sub> electrode, which can be attributed to the formation of an SEI film.

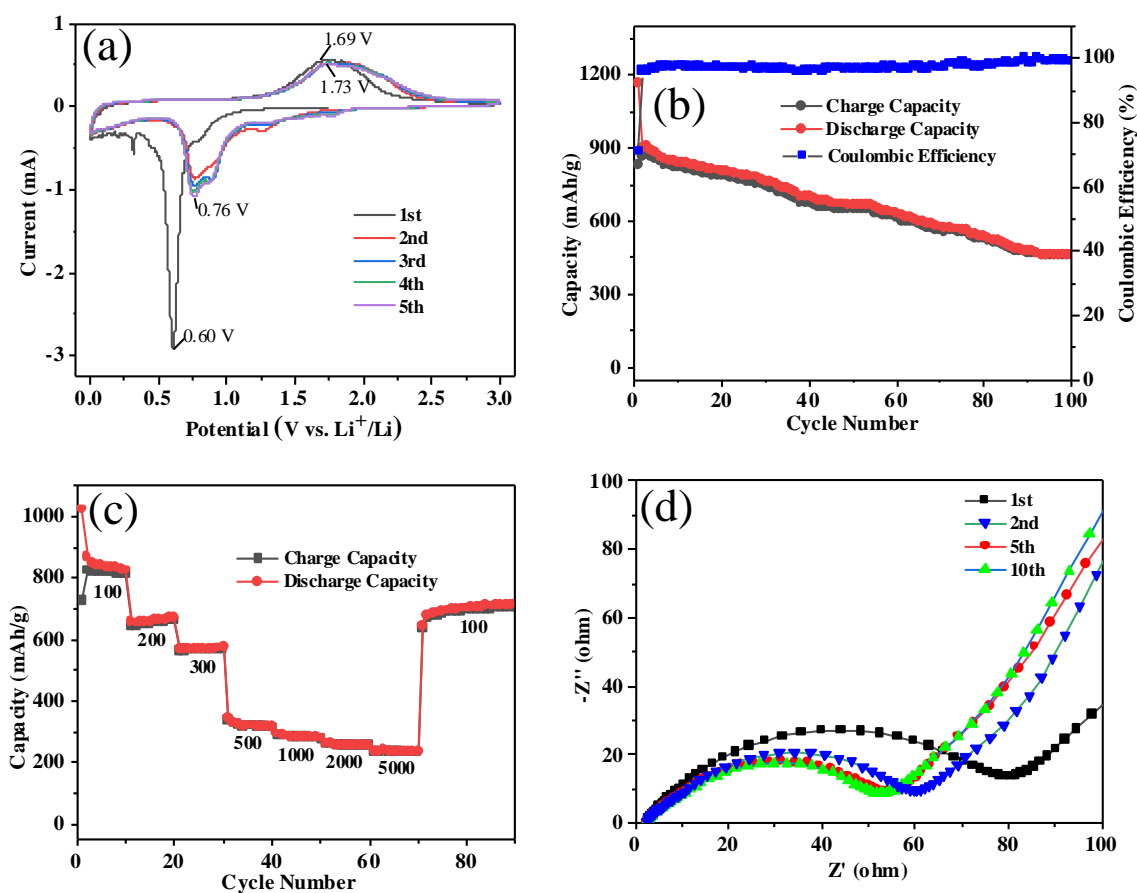


**Figure 3.** (a) Cyclic voltammogram of the anemone-shaped Fe<sub>3</sub>O<sub>4</sub> electrode at a scan rate of 0.1 mV s<sup>-1</sup> (b) Cycling performance and the Coulombic efficiency of the anemone-shaped Fe<sub>3</sub>O<sub>4</sub> at a current density of 100 mA g<sup>-1</sup>; (c) The rate performance of the anemone-shaped Fe<sub>3</sub>O<sub>4</sub>; and (d) Impedance spectra of the anemone-shaped Fe<sub>3</sub>O<sub>4</sub> after some electrochemical cycles.

Fig. 3 (b) depicts the long cycling performance of the anemone-shaped Fe<sub>3</sub>O<sub>4</sub> electrode along with the Coulombic efficiency at a current density of 100 mA g<sup>-1</sup>. The reversible capacity of the first cycle was 1166 mAh g<sup>-1</sup>. Normally, pure-phase Fe<sub>3</sub>O<sub>4</sub> materials exhibit poor capacity retention [6]. However, the charge/discharge capacity of the anemone-shaped Fe<sub>3</sub>O<sub>4</sub> electrode changed slightly and was maintained at 552/556 mAh g<sup>-1</sup> during the 100<sup>th</sup> cycle with a Coulombic efficiency of 99%. The electrode exhibited a good cycle life, indicating the stable construction of anemone-shaped Fe<sub>3</sub>O<sub>4</sub> micro-structures, which decreases the strain aggregation of active materials during the charge–discharge [17]. In addition, the Coulombic efficiency of anemone-shaped Fe<sub>3</sub>O<sub>4</sub> micro-structures was only 71% in the first cycle, which increased rapidly to 99% after several cycles. Furthermore, the anemone-shaped Fe<sub>3</sub>O<sub>4</sub> micro-structures electrode exhibited good rate performance. Fig. 3 (c) shows that the anemone-shaped Fe<sub>3</sub>O<sub>4</sub> electrode delivered reversible capacities of 1022, 658, 567, 344, 293, 263 and 236 mAh g<sup>-1</sup> at current densities of 100, 200, 300, 500, 1000, 2000 and 5000 mA g<sup>-1</sup>, respectively. The discharge capacity recovered to 716 mAh g<sup>-1</sup> at the 90<sup>th</sup> cycle when the current density returned to 100 mA g<sup>-1</sup>. The performance of anemone-shaped Fe<sub>3</sub>O<sub>4</sub> micro-structures was compared with similar anode materials reported in the previous work in (Table 1). The comparison showed that the anemone-shaped Fe<sub>3</sub>O<sub>4</sub> micro-structure is a promising anode material for Li-ion batteries with a long-term cycling stability.

**Table 1.** Initial discharge capacity and discharge capacity after cycling of various iron oxides reported in the literature.

Anode materials	Current density	Initial discharge capacity (mAh g <sup>-1</sup> )	Cycle number	Remaining capacity (mAh g <sup>-1</sup> )	Ref.
Fe <sub>3</sub> O <sub>4</sub> nano-belt	500 mA g <sup>-1</sup>	1090	60	404	[18]
Spherical Fe <sub>3</sub> O <sub>4</sub>	0.2C	1307	110	450	[19]
Fe <sub>3</sub> O <sub>4</sub> nano-flakes	100 mA g <sup>-1</sup>	1380	20	96	[20]
Fe <sub>3</sub> O <sub>4</sub> hexa-hedra	100 mA g <sup>-1</sup>	1303	40	644	[21]
Fe <sub>3</sub> O <sub>4</sub> nano-cages	200 mA g <sup>-1</sup>	1086	100	876	[22]
Fe <sub>3</sub> O <sub>4</sub> @C@NS-rGO	100 mA g <sup>-1</sup>	2028.6	100	532.5	[23]
Fe <sub>3</sub> O <sub>4</sub> octa-hedra	50 mA g <sup>-1</sup>	1077	38	365	[24]
Anemone-shaped Fe <sub>3</sub> O <sub>4</sub>	100 mA g <sup>-1</sup>	1166	100	556	this work

EIS of anemone-shaped Fe<sub>3</sub>O<sub>4</sub> was tested for identifying the rate capability of anemone-shaped Fe<sub>3</sub>O<sub>4</sub> micro-structures in the range of 100 kHz–0.01 Hz. As shown in Fig. 3 (d), the diameter of the semi-circle was small in the high-frequency region, indicating the good transport capacity of electrons. The diagonal line exhibits the diffusion ability of Li<sup>+</sup> in the low-frequency region. The resistance of the electrode–electrolyte interfaces (R<sub>ct</sub>) of the anemone-shaped Fe<sub>3</sub>O<sub>4</sub> electrode after discharging for some cycles (1<sup>st</sup>, 2<sup>nd</sup>, 5<sup>th</sup> and 10<sup>th</sup>) were ~80, ~60, ~55 and ~ 52 Ω, respectively. The impedance decreased, possibly because of the electrochemical milling effect [25]. Overall, EIS showed

that the anemone-shaped Fe<sub>3</sub>O<sub>4</sub> electrode exhibits good rate capability.

#### 4. CONCLUSIONS

Anemone-shaped Fe<sub>3</sub>O<sub>4</sub> micro-structures were assembled from nano-rods using a facile solvothermal method. The anemone-shaped Fe<sub>3</sub>O<sub>4</sub> electrode exhibited a reversible capacity of 1166 mAh g<sup>-1</sup> in the first cycle and 556 mAh g<sup>-1</sup> at 100 cycles at a current density of 100 mA g<sup>-1</sup> with relatively good rate capability. The pure-phase anemone-shaped Fe<sub>3</sub>O<sub>4</sub> micro-structures exhibited improved electrochemical performance and can be used as a practical promising anode materials for Li-ion batteries.

#### ACKNOWLEDGMENTS

This study was supported by the Key R & D project of Shandong Province (No. 2019GSF111042) and the Major agricultural application technology innovation project in Shandong Province (2018).

#### References

1. Q. X. Xie, Y. F. Zhang, D. L. Xie, P. Zhao, *J. Electroanal. Chem.*, 857 (2020) 113749.
2. Q. C. Wu, R. L. Jiang, L. X. Mu, S. Y. Xu. *C. R. Chimie*, 22 (2019) 96-102.
3. H. Liu, G. Wang, J. Wang, D. Wexler, *Electrochem. Commun.*, 10 (2008) 1879-1882.
4. M. Choi, S. H. Lee, Y. I. Jung, J. J. Jung, J. S. Park, W. K. Choi, S. Y. Park, H. J. Won, J. K. Moon, J. Choi, S. B. Kim, *J. Alloys Compd.*, 729 (2017) 802-808.
5. K. L. Wu, M. Ling, P. Y. Zeng, L. Zhang, T. Wu, P. L. Guan, W. C. Cheng, Z. Chen, Z. Fang, X. W. Wei, *Sci. China Mater.*, 64 (2021) 1058.
6. M. Choi, S. H. Lee, Y. I. Jung, W. K. Choi, J. K. Moon, J. Choi, B. K. Seo, S. B. Kim, *Electron. Mater.*, 19, (2018) 417-422.
7. J. C. Ma, J. L. Chang, H. Z. Ma, D. D. Zhang, Q. L. Ma, S. B. Wang, *J. Colloid Interface Sci.*, 498 (2017) 282-291.
8. S. Q. Wang, J. Y. Zhang, C. H. Chen, *J. Power Sources*, 195 (2010) 5379-5381.
9. J. X. Yao, K. Zhang, W. Wang, X. Q. Zuo, Q. Yang, H. B. Tang, M. Z. Wu, G. Li, *ACS Appl. Mater. Interfaces*, 10 (2018), 19564-19572.
10. H. S. Lim, B. Y. Jung, Y. K. Sun, K. D. Suh, *Electrochim. Acta*, 75 (2012) 123-130.
11. Z. Yang, D. Y. Su, J. P. Yang, J. Wang, *J. Power Sources*, 363 (2017) 161-167.
12. J. J. Ye, Q. Hao, B. B. Liu, Y. P. Li, C. X. Xu, *Chem. Eng. J.*, 315 (2017) 115-123.
13. X. Jiang, X. L. Yang, Y. H. Zhu, Y. F. Yao, P. Zhao, C. Z. Li, *J. Mater. Chem. A3* (2015) 2361-2369.
14. L. H. Wang, L. L. Ren, Y. F. Qin, J. Chen, H. Y. Chen, K. Wang, H. J. Liu, Z. Huang, Q. Li, *Int. J. Electrochem. Sci.*, 17 (2022) 220221.
15. S. R. Kumar, J. G. Kim, C. Viswanathan, W. B. Kim, R. K. L. Selvan, N. Ponpandiana, *Mater. Res. Bull.*, 97 (2018) 272-280.
16. H. Lv, Y. Q. Xue, X. H. Feng, H. X. Wang, M. Zheng, B. Y. Zhang, *Int. J. Electrochem. Sci.*, 15 (2020) 2157-2165.
17. J. Luo, J. Liu, Z. Zeng, C. F. Ng, L. Ma, H. Zhang, J. Lin, Z. Shen, H. J. Fan, *Nano Lett.*, 13 (2013) 6136-6143.
18. Y. Shi, M. M. Shi, H. Z. Chen, Y. Q. Qiao, J. P. Tu, *Nanotechnology*, 23 (2012) 395601.
19. J. S. Xu, Y. J. Zhu, *ACS Appl. Mater. Interfaces*, 4 (2012) 4752-4757.

20. X. Lou, J. Huang, T. Li, H. Hu, B. Hu, Y. J. Zhang, *Mater. Sci.: Mater. Electron.*, 25 (2014) 1193-1196.
21. Q. Wang, D. Chen, J. Chen, C. Lai, L. Li, C. Wang, *Mater. Lett.*, 141 (2015) 319-322.
22. T. Xia, X. L. Xu, J. P. Wang, C. B. Xu, F. C. Meng, Z. Shi, J. Lian, J. M. Bassat, *Electrochim. Acta*, 160 (2015) 114-122.
23. X. F. Chen, X. Y. Zhu, G. P. Cao, S. T. Zhang, Y. Mu, H. Ming, J. Y. Qiu, *Energy Fuels*, 35 (2020) 1810-1819.
24. S. Jia, T. T. Song, B. G. Zhao, Q. J. Zhai, Y. L. Gao, *J. Alloys Compd.*, 617 (2014) 787-791.
25. D. W. Zhang, C. H. Chen, J. Zhang, F. Ren, *Chem. Mater.*, 17 (2005) 5242-5245.

© 2022 The Authors. Published by ESG ([www.electrochemsci.org](http://www.electrochemsci.org)). This article is an open access article distributed under the terms and conditions of the Creative Commons Attribution license (<http://creativecommons.org/licenses/by/4.0/>).